Lattice Response Functions of Imperfect Crystals: Effects Due to a Local Change of Mass and Short-Range Interaction*

G. BENEDEK AND G. F. NARDELLI†
Istituto di Fisica dell'Università di Milano, Milano, Italy
(Received 15 August 1966)

Lattice response functions, such as the thermal conductivity and dielectric susceptibility of an imperfect crystal with rocksalt structure, are evaluated in terms of the irreducible T matrix accounting for the phonon scattering. It is shown that the effect of defects on thermal conductivity and dielectric susceptibility can be accounted for by expressions which have essentially the same structure. The T matrix for a defect which affects both the mass and the short-range interaction is analyzed according to the irreducible representations of the point group which pertains to the perturbation, and the resonance conditions for Γ_1, Γ_{12}, and Γ_{15} irreducible representations are considered in detail for any positive impurity in KBr crystals. Hardy's deformation-dipole (DD) model is employed for the description of the host-lattice dynamics. A comparison is made with simplified models, such as diatomic linear chains with nearest-neighbor interaction; it is shown that in polar crystals an effective-force constant has to be used in order to give a reliable description of the short-range interaction between the impurity and the host lattice. An attempt is made to define such effective force constants in the framework of the DD model. The numerical calculations concern positive monovalent impurities in KBr crystals. Γ_1, Γ_{12}, and Γ_{15} resonance frequencies are evaluated as a function of the change of mass and nearest-neighbor force constant. For KBr:Li^+ and KBr:Ag^+ we also evaluate the band shape of the absorption spectrum at infrared frequencies; good agreement is found between the theoretical prediction and the experimental data on KBr:Li^+. It is shown that some structures actually observed in the spectrum are due to peaks in the projected density of states of the host lattice, and have nothing to do with resonance scattering. Good agreement is found between the impurity-host-lattice interaction as estimated from *a priori* calculations and as deduced by fitting the Γ_{15} resonance frequency to the experimental data. A simple explanation of the off-center position of small ions is also suggested. Finally, concentration and stress effects on the absorption coefficient are briefly discussed.

I. INTRODUCTION

RECENTLY, attention has been called to the response that an imperfect crystal gives under the action of an external disturbance, such as electromagnetic[1–3] and neutron[4] radiations or thermal gradients.[5,6] It is well known that the peculiarities these response functions display in the range of the phonon frequencies are to be ascribed to the defect-induced phonon scattering.[7]

The model which has been used till now to account for the effects of the defect-induced phonon scattering was essentially a pure change of mass. This model was useful for recognizing that the peaks which might occur at the high-frequency side of the *Reststrahlen* frequency are effects due to the eventual local modes induced by the defect. However, this model did not allow for a good interpretation of the peaks that sometimes are observed at the low-frequency side.[2,3]

The effect that a local change of force constant has on the imperfect-lattice dynamics has been discussed qualitatively by several authors[8–10] on the basis of oversimplified models, such as linear chains with nearest-neighbor (n.n.) interaction. Recently, it was stressed by one of the present authors that the change in the short-range interaction can play an essential role in the quantitative explanation of the experimental data.[11] In the present paper we try to perform a realistic calculation on a substitutional impurity in lattices having rocksalt structure, and to predict the effects on the response functions.

In order to do this, we have developed the imperfect-lattice dynamics on the basis of the T-matrix formalism, and have analyzed the T matrix according to the irreducible representations (irr.rep.) of the point group which pertains to the perturbation. This is done in Sec. II, where the properties of the T matrix are also examined in the complex z plane. With the aim of shedding some light on the local interaction around an impurity ion, an attempt is made (see Sec. III) to define an effective-force constant for the (n.n.) interaction in ionic crystals. The expression for the response functions of the imperfect crystal is considered in Sec. IV. There, their dependence on the T matrix of a single defect is

* This research has been sponsored in part by the European Office of Aerospace Research, U. S. Air Force under Grant N.65-05.

† Italian National Council for Research, Gruppo Nazionale di Struttura della Materia.

[1] G. Schaefer, J. Phys. Chem. Solids, **12**, 233, (1960).

[2] A. J. Sievers, Phys. Rev. Letters, **13**, 310 (1964).

[3] A. J. Sievers, A. A. Maradudin, and S. S. Jaswal, Phys. Rev. **138**, A272 (1965).

[4] B. Mozer, K. Otnes, and V. W. Myers, Phys. Rev. Letters **8**, 278 (1962).

[5] R. Berman, Advan. Phys. **2**, 103 (1953).

[6] C. T. Walker and R. O. Pohl, Phys. Rev. **131**, 1433 (1963).

[7] A general survey and an extensive bibliography on theoretical studies on these topics are given in A. A. Maradudin, in *Solids State Physics*, edited by F. Seitz and D. Turnbull (Academic Press Inc., New York, 1966), Vols. 18 and 19.

[8] See, for example, W. Ludwig, Ergebn. Exakt. Naturwiss. **31**, 1 (1964).

[9] A. J. Sievers and S. Takeno, Phys. Rev. **140**, A1030 (1965).

[10] L. Genzel, K. F. Renk, and R. Weber, Phys. Status Solidi **12**, 639 (1965).

[11] R. Fieschi, G. F. Nardelli, and N. Terzi, Phys. Rev. **138**, A203 (1965).

fully explained. The emphasis is given to the complex dielectric susceptibility; it is shown that to lowest order in the concentration only T_{OO}, the optic-active element of the scattering matrix, is involved. T_{OO} is evaluated in Sec. IV on the basis of a model which accounts for both changes of mass and (n.n.) force constant.

Finally, the conditions for resonance scattering of Γ_{15} (the optic-active) as well as Γ_1 and Γ_{12} (the Raman-active) symmetry modes are analyzed in Sec. V, where the numerical results for impurities in a KBr host lattice are reported and compared with the experimental results for KBr:Li^+ [9] and KBr:Ag^+.[2] The extension to a change in both central and noncentral force constants is outlined in the Appendix. The numerical results for defects in KI were reported elsewhere,[12] while the systematic analysis of the resonance conditions for defects in several other host lattices will be presented in a subsequent paper.

II. T-MATRIX FORMALISM

Consider a crystal containing a number of defects of the same kind with finite concentration p, and let $\mathbf{x}_1$, $\mathbf{x}_2$, $\cdots$, $\mathbf{x}_j$, $\cdots$, $\mathbf{x}_{pN}$ (where N is the number of primitive cells comprising the crystal) be the set of lattice vectors which characterizes a given configuration, say A, of defects. The mass matrix of the imperfect lattice can be written as

$$\mathbf{M}_A=\mathbf{M}_0[\mathbf{I}-\epsilon\boldsymbol{\Delta}_A]. \tag{1}$$

$\mathbf{M}_0$ is the mass matrix of the perfect lattice, $-\epsilon$ is the fractional change of mass due to a single defect, and $\boldsymbol{\Delta}_A$ is the matrix whose components in the lattice-displacement representation are given by

$$\Delta_{A,xy}(l,l')\equiv\delta_{xy}\textstyle\sum_j{}^{(A)}\delta_{lj}\delta_{l'j}. \tag{2}$$

In expression (2), x and y denote Cartesian components, index l labels the lattice vectors $\mathbf{x}_l\equiv\mathbf{x}_l+\mathbf{x}_\kappa$ ($\mathbf{x}_l$=Bravais vector, $\mathbf{x}_\kappa$=site vector in the primitive cell), and the summation runs over the set of lattice sites which characterizes the configuration (A) of defects. As usual, δ_{lj} and δ_{xy} are Kronecker symbols. A subscript A has been added to $\mathbf{M}$ on the left-hand side of Eq. (1) and to $\boldsymbol{\Delta}$ in order to emphasize that these matrices depend on the configuration of defects. The force-constant matrix of the imperfect lattice can be split as

$$\boldsymbol{\Phi}_A=\boldsymbol{\Phi}_0+\delta\boldsymbol{\Phi}_A, \tag{3}$$

where $\boldsymbol{\Phi}_0$ refers to the perfect lattice, and the normal-mode equation reads

$$[\mathbf{L}_0+\boldsymbol{\Lambda}_A(\omega^2)]\psi_\lambda=\omega_\lambda{}^2\psi_\lambda, \tag{4}$$

where ω_λ is a normal-mode frequency of the imperfect lattice.

$$\boldsymbol{\Lambda}_A(\omega^2)\equiv\mathbf{M}_0{}^{-1/2}\delta\boldsymbol{\Phi}_A\mathbf{M}_0{}^{-1/2}+\epsilon\omega^2\boldsymbol{\Delta}_A=\boldsymbol{\Lambda}_A+\epsilon\omega^2\boldsymbol{\Delta}_A, \tag{5}$$

is the frequency-dependent perturbation, and $\mathbf{L}_0$ is the dynamical matrix of the perfect lattice.

In considering Eq. (4) it is understood that the normal modes ψ_λ satisfy the orthonormality condition

$$(\psi_\lambda,[\mathbf{I}-\epsilon\boldsymbol{\Delta}_A]\psi_{\lambda'})=\delta_{\lambda\lambda'}, \tag{6}$$

which assures the equivalence between Eq. (4) and the more "natural" normal-mode equation

$$\mathbf{L}_A\psi_\lambda{}'=\omega_\lambda{}^2\psi_\lambda', \tag{7}$$

where $\mathbf{L}_A\equiv\mathbf{M}_A{}^{-1/2}(\boldsymbol{\Phi}_0+\delta\boldsymbol{\Phi}_A)\mathbf{M}_A{}^{-1/2}$ is the dynamical matrix of the imperfect lattice.[11]

In the lattice-displacement representation $\boldsymbol{\Lambda}_A(\omega^2)$ reads

$$\Lambda_{A,xy}(l,l';\omega^2)=\textstyle\sum_j{}^{(A)}\{\Lambda_{xy}(l-j,l'-j)+\epsilon\omega^2\Delta_{xy}(l-j,l-j')\}, \tag{8}$$

where

$$\Lambda_{xy}(l,l')=\mathbf{M}_0{}^{-1/2}(l)\delta\boldsymbol{\Phi}_{xy}(l,l')\mathbf{M}_0{}^{-1/2}(l'),$$

and $\epsilon\omega^2\Delta_{xy}(l,l')$ account, respectively, for the change of force constants and for the change of mass due to a single defect at the origin of the crystallographic axes.[11] It will be shown in the following sections that both the thermal- and the optical-response functions of an imperfect lattice can be expressed, in harmonic approximation, in terms of the inverse matrix

$$\langle(\mathbf{L}_0+\boldsymbol{\Lambda}_A(\omega^2)-z)^{-1}\rangle_{\mathrm{av}}, \tag{9}$$

where the brackets with the subscript av denote a statistical average over all the configurations of defects with the same concentration p, and $z=\omega^2+i\eta$ is the complex squared frequency.

We define now a T matrix for the total system of defects by the equation

$$\mathbf{T}_A(z)=\boldsymbol{\Lambda}_A(\omega^2)-\boldsymbol{\Lambda}_A(\omega^2)(\mathbf{L}_0-z)^{-1}\mathbf{T}_A(z), \tag{10a}$$

or

$$\mathbf{T}_A(z)=\boldsymbol{\Lambda}_A(\omega^2)-\mathbf{T}_A(z)(\mathbf{L}_0-z)^{-1}\boldsymbol{\Lambda}_A(\omega^2), \tag{10b}$$

which has the formal solution

$$\mathbf{T}_A(z)=\boldsymbol{\Lambda}_A(\omega^2)[\mathbf{I}+(\mathbf{L}_0-z)^{-1}\boldsymbol{\Lambda}_A(\omega^2)]^{-1} \tag{11a}$$

or

$$\mathbf{T}_A(z)=[\mathbf{I}+\boldsymbol{\Lambda}_A(\omega^2)(\mathbf{L}_0-z)^{-1}]^{-1}\boldsymbol{\Lambda}_A(\omega^2). \tag{11b}$$

$\mathbf{T}_A(z)$ accounts for the multiple scattering of lattice waves in which one, two, three, etc., defects are involved at a time. The contributions to $\mathbf{T}_A(z)$ can be analyzed by a diagram technique. We use the wave-vector representation $(\mathbf{q},s)\equiv q$, where $\mathbf{q}$ is a wave vector and s is the branch index; following Langer,[13] a horizontal line with label q (phonon line) represents the free normal-mode

[12] G. Benedek and G. F. Nardelli, in Proceedings of the Conference on Calculations of the Properties of Vacancies and Interstitials, Skiland, Virginia, 1966 (to be published).

[13] J. S. Langer, J. Math. Physics, 2, 584 (1961).

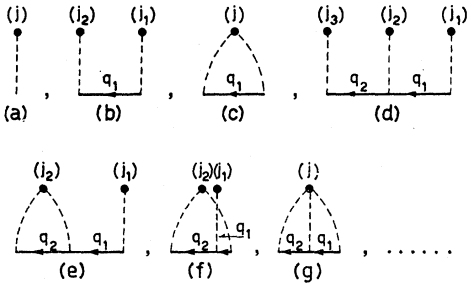

FIG. 1. Graphs entering the expansion of the perturbed Green's function. (a), (c), (f), and (g) are irreducible graphs.

Green's function

$$G_q(z)\equiv(\omega^2{}_j(\mathbf{q})-z)^{-1}; \tag{12}$$

the interactions are denoted by dashed lines which start from dots representing the defect sites where interactions occur and connect to the phonon line in the order in which they occur in the perturbation expansion of (11a) or (11b). The graphs entering $\mathbf{T}_A(z)$ are of the type shown in Fig. 1.

It has been shown by Langer[13,14] that the statistical average makes the inverse matrix (9) expressible in terms of the irreducible part, say $\mathbf{T}_{A,\mathrm{irr}}(z)$, of the T matrix. It turns out that

$$\langle(\mathbf{L}_0+\mathbf{\Lambda}_A(\omega^2)-z)^{-1}\rangle_{\mathrm{av}}=(\mathbf{L}_0+\langle\mathbf{T}_{A,\mathrm{irr}}(z)\rangle_{\mathrm{av}}-z)^{-1}, \tag{13}$$

where $\mathbf{T}_{A,\mathrm{irr}}(z)$ is defined as the sum of all the irreducible graphs entering the perturbation expansion of the T matrix. Here, we call irreducible a graph which cannot be separated into two disconnected parts by breaking a single phonon line. [In Fig. 1, (a), (c), (f), and (g) are irreducible graphs.] $\langle\mathbf{T}_{A,\mathrm{irr}}(z)\rangle_{\mathrm{av}}$ is recognized to be a diagonal matrix with respect to wave-vector indices.

Consider the T matrix $\mathbf{T}_1(z)$ for a single defect and perform the statistical average over a single-defect random distribution with probability p at every site of the Bravais lattice. We define a matrix $\mathbf{T}(z)$ by

$$p\mathbf{T}(z)=\langle\mathbf{T}_1(z)\rangle_{\mathrm{av}}. \tag{14}$$

$\mathbf{T}(z)$ is recognized to be a matrix which is diagonal in the wave-vector representation and has finite matrix elements. In the approximation in which only repeated scattering of a lattice wave by the same defect is considered in summing up irreducible graphs, it turns out that

$$\langle\mathbf{T}_{A,\mathrm{irr}}(z)\rangle_{\mathrm{av}}=p\mathbf{T}(z). \tag{15}$$

Further contributions to $\langle\mathbf{T}_{A,\mathrm{irr}}(z)\rangle_{\mathrm{av}}$ involve polynomials of second and higher order in the defect concentration. To lowest order in p, expression (9) can be written finally as

$$\langle(\mathbf{L}_0+\mathbf{\Lambda}_A(\omega^2)-z)^{-1}\rangle_{\mathrm{av}}=(\mathbf{L}_0+p\mathbf{T}(z)-z)^{-1}, \tag{16}$$

and it is seen to involve the T matrix for the single defect $\mathbf{T}(z)$.

We consider now in more detail the T matrix for a single defect. The inspection of expression (11a) or (11b), with the suffix A dropped, tells us that the matrix $\mathbf{T}_1(z)$ has the same rank and symmetry as the matrix $\mathbf{\Lambda}(\omega^2)$; thus, $\mathbf{T}_1(z)$ can be analyzed according to the irr.reps., say Γ, of the point group which pertains to the perturbation itself. Let $|\Gamma,j)$ denote the oriented symmetry vectors in the subspace where the perturbation has nonvanishing matrix elements, which transforms according to the first row of the irr. rep. Γ. The label j runs from 1 to $n(\Gamma)$, where $n(\Gamma)$ is the number of times Γ occurs in $\mathbf{\Lambda}(\omega^2)$. $\mathbf{T}_1(z)$ can be written as

$$\mathbf{T}_1(z)=\sum_\Gamma\sum_{jj'}|\Gamma,j)(\Gamma,j|\mathbf{T}_1(z)|\Gamma,j')(\Gamma,j'|. \tag{17}$$

A. Defects in Rocksalt Structures

We assume that the defect affects the mass and the n.n. force constant of central type, say f, with the point symmetry of the lattice; it is then an easy matter to verify that the irr.rep. Γ of the full cubic group appears in our $\mathbf{\Lambda}(\omega^2)$ $n(\Gamma)$ times as follows:

$$\begin{aligned} &n(\Gamma_1)=1, \quad n(\Gamma_{15})=3, \quad n(\Gamma_{25})=1, \\ &n(\Gamma_{12})=1, \quad n(\Gamma_{15}')=1, \quad n(\Gamma_{25}')=1, \end{aligned} \tag{18}$$

and that the nonvanishing matrix elements of $\mathbf{\Lambda}(\omega^2)$ are

$$(\Gamma_1|\mathbf{\Lambda}(\omega^2)|\Gamma_1)=\tfrac{1}{2}\chi\lambda, \tag{19a}$$

$$(\Gamma_{12}|\mathbf{\Lambda}(\omega^2)|\Gamma_{12})=\tfrac{1}{2}\chi\lambda, \tag{19b}$$

and

$$(\Gamma_{15},j|\mathbf{\Lambda}(\omega^2)|\Gamma_{15},j')=\begin{pmatrix}\lambda+\epsilon\omega^2 & -(\chi/2)^{1/2}\lambda\\ -(\chi/2)^{1/2}\lambda & \lambda+\epsilon\omega^2\end{pmatrix}. \tag{19c}$$

Notice that irr.reps. Γ_{15}', Γ_{25}, and Γ_{25}' enter $\mathbf{\Lambda}(\omega^2)$ with vanishing matrix elements and that irr.rep. Γ_{15} enters with a 2×2 instead of a 3×3 matrix, because the noncentral force constant has been disregarded.

In the above expressions $\chi\equiv M(\pm)/M(\mp)$ denotes the host-crystal mass ratio, while $\lambda=\Delta f/M(\pm)$ denotes the change of the n.n. force constant in units of a squared frequency. We have labeled the two sublattices of our crystal with a plus or minus sign; the choice of the upper or lower sign depends on whether the impurity lies at the positive or negative sublattice. The projected Green's functions $(\Gamma,j|(\mathbf{L}_0-z)^{-1}|\Gamma,j')$ are found to have the following matrix elements:

$$(\Gamma_1|(\mathbf{L}_0-z)^{-1}|\Gamma_1)=2[\mathcal{G}_4{}^{\pm}(z)+2\mathcal{G}_5{}^{\pm}(z)], \tag{20a}$$

$$(\Gamma_{12}|(\mathbf{L}_0-z)^{-1}|\Gamma_{12})=2[\mathcal{G}_4{}^{\pm}(z)-\mathcal{G}_5{}^{\pm}(z)], \tag{20b}$$

and

$$(\Gamma_{15},j|(\mathbf{L}_0-z)^{-1}|\Gamma_{15},j')=\begin{pmatrix}\mathcal{G}_1{}^{\pm}(z) & 2^{1/2}\mathcal{G}_2{}^{\pm}(z)\\ 2^{1/2}\mathcal{G}_2{}^{\pm}(z) & 2\mathcal{G}_3{}^{\pm}(z)\end{pmatrix}. \tag{20c}$$

$\mathcal{G}_\mu{}^{\pm}(z)$, $\mu=1,2,3,4,5$, denotes the complex-valued in-

[14] A. A. Maradudin, in *Astrophysics and the Many-Body Problem* (W. A. Benjamin, Inc., New York, 1963), Vol. 2, pp. 107–320.

tegrals over the Brillouin zone (BZ):

$$\mathcal{G}_\mu^{\pm}(z)=v\sum_{s=1}^{6}\int^{BZ} d\mathbf{q}\; j_\mu^{\pm}(\mathbf{q},s)(\omega^2_{\mathbf{q},s}-z)^{-1}, \quad (21)$$

where $j_\mu^{\pm}(\mathbf{q},s)$ have the following expressions:

$$j_1^{\pm}(\mathbf{q},s)=e_x^2(\pm|\mathbf{q},s) \quad (22a)$$

$$j_2^{\pm}(\mathbf{q},s)=e_x(\pm|\mathbf{q},s)e_x(\mp|\mathbf{q},s)\cos(2\pi r_0 q_x), \quad (22b)$$

$$j_3^{\pm}(\mathbf{q},s)=e_x^2(\mp|\mathbf{q},s)\cos^2(2\pi r_0 q_x), \quad (22c)$$

$$j_4^{\pm}(\mathbf{q},s)=e_x^2(\mp|\mathbf{q},s)\sin^2(2\pi r_0 q_x), \quad (22d)$$

$$j_5^{\pm}(\mathbf{q},s)=e_y(\mp|\mathbf{q},s)e_z(\mp|\mathbf{q},s)\sin(2\pi r_0 q_y)\sin(2\pi r_0 q_z). \quad (22e)$$

Here v is the volume of the primitive cell, r_0 is the n.n. distance, and $e_x(\pm|\mathbf{q},s)$ is the xth Cartesian component of the polarization vector of the lattice wave $(\mathbf{q},s)$.

By use of (19) and (20), expression (11) can be handled with no particular d fficulty, and the irr.rep. $\mathbf{T}^{(\Gamma)}(z)$ of the T matrix for the defect we have considered are found in the form

$$\mathbf{T}^{(\Gamma)}(z)=\mathbf{N}^{(\Gamma)}(z)/D^{(\Gamma)}(z), \quad (23)$$

where the numerator, say $\mathbf{N}^{(\Gamma)}$, is given by

$$\mathbf{N}^{(\Gamma_1)}=\tfrac{1}{2}\chi\lambda, \quad (24a)$$

$$\mathbf{N}^{(\Gamma_{12})}=\tfrac{1}{2}\chi\lambda,$$

and

$$\mathbf{N}^{(\Gamma_{15})}=\begin{pmatrix}\lambda+\epsilon\omega^2(1+\chi\lambda\mathcal{G}_3^{\pm}(z)) & -(\tfrac{1}{2}\chi)^{1/2}\lambda(1+\chi^{1/2}\epsilon\omega^2\mathcal{G}_2^{\pm}(z))\\ -(\tfrac{1}{2}\chi)^{1/2}\lambda(1+\chi^{1/2}\epsilon\omega^2\mathcal{G}_2^{\pm}(z)) & (\tfrac{1}{2}\chi)\lambda(1+\epsilon\omega^2\mathcal{G}_1^{\pm}(z))\end{pmatrix}, \quad (24b)$$

while the denominator, say $D^{(\Gamma)}$, is found to have the following expression:

$$D^{(\Gamma_1)}=1+\chi\lambda(\mathcal{G}_4^{\pm}(z)+2\mathcal{G}_5^{\pm}(z)), \quad (25a)$$

$$D^{(\Gamma_{12})}=1+\chi\lambda(\mathcal{G}_4^{\pm}(z)-\mathcal{G}_5^{\pm}(z)), \quad (25b)$$

and

$$D^{(\Gamma_{15})}=1+\epsilon\omega^2\mathcal{G}_1^{\pm}(z)+\lambda[\mathcal{G}_1^{\pm}(z)+\chi\mathcal{G}_3^{\pm}(z)-2\chi^{1/2}\mathcal{G}_2^{\pm}(z)]+\epsilon\omega^2\lambda\chi[\mathcal{G}_1^{\pm}(z)\mathcal{G}_3^{\pm}(z)-\mathcal{G}_2^{\pm 2}(z)]. \quad (25c)$$

It appears that the numerator is, in the general case, a complex matrix of rank equal to the number of times the Γ irr.rep. enters by nonvanishing matrix elements the perturbation $\mathbf{\Lambda}(\omega)$, while the denominator is a complex function of the complex squared frequency z.

Since, upon letting the imaginary part of z go to zero, the last factor in the integrand of the defining expression (21) of $\mathcal{G}_\mu^{\pm}(z)$ is seen to approach a representation of the δ_+ or δ_- function, depending on whether z approaches the real axis from the upper or the lower half plane, the BZ integrals $\mathcal{G}_\mu^{\pm}(z)$ and, therefore, the denominator and eventually the numerator of $\mathbf{T}^{(\Gamma)}(z)$ are recognized to be multivalued functions of the complex squared frequency z. The branch cuts lie on the real axis of the complex z plane and occur along every frequency interval where the spectral density of the lattice waves assumes finite values.

Split the BZ integral $\mathcal{G}_\mu(z)$ into real and imaginary parts (we drop for the moment the superscript $\pm$ on $\mathcal{G}_\mu$). In the limit $z=\omega^2+i\eta$ with $\eta=0^+$, it is an easy matter to verify [see expression (21)] that the real part, say $\mathcal{G}_\mu^{(1)}(\omega^2)$, never vanishes, while the imaginary part approaches either a finite nonvanishing value, say $\mathcal{G}_\mu^{(2)}(\omega^2)$, or an infinitesimal value, say $\eta\bar{G}_\mu(\omega^2)$, depending on whether ω is, or is not, a frequency of the vibrational continuum. Hereafter we use the term "vibrational continuum" for the frequency interval (or intervals, if a forbidden frequency gap occurs) which corresponds to the vibrational spectrum of the perfect lattice. On taking this property of $\mathcal{G}_\mu(\omega^2)$ into account, inspection of (23), (24), and (25) tells us that both real and imaginary parts of $\mathbf{T}^{(\Gamma)}(z)$ approach finite values, as z approaches the real axis at a point ω^2 of the vibrational continuum, while $\mathbf{T}^{(\Gamma)}(z)$ exhibits a singularity at every point of the real axis outside the vibrational continuum where the real part of its denominator vanishes.

The T matrix we have here considered has been introduced by looking at the time-independent equation for the perturbed normal modes [see Eq. (7)], rather than one-phonon states. Nevertheless, it can be shown[15] that our T matrix corresponds again to a scattering process with the appropriate initial and final conditions, provided we consider the limit $z=\omega^2+i0^+$. In what follows we denote by $\mathbf{T}^{(\Gamma)}(\omega^2)$ the limit

$$\mathbf{T}^{(\Gamma)}(\omega^2)=\lim_{\eta\to 0^+}\mathbf{T}^{(\Gamma)}(\omega^2+i\eta)\equiv\mathbf{T}_1^{(\Gamma)}(\omega^2)+i\mathbf{T}_2^{(\Gamma)}(\omega^2). \quad (26)$$

Resonant scattering is said to occur when $\mathrm{Re}D^{(\Gamma)}(\omega^2)=0$.

Since the time-dependent equation for the normal modes involves a second-order, rather than first-order, time derivative, our T matrix has not the same meaning as in quantum-scattering theory. Indeed, it is an easy matter to verify[16] that the argument $\delta^{(\Gamma)}(\omega)$ of the resonance denominator $D^{(\Gamma)}(\omega^2)$ appearing in (23) represents, to within a factor π, the fractional shift of squared frequency induced by the scattering. In this sense the T-matrix approach contains the early Lifshitz theory.

Expressions (23), (24), and (25) give the T matrix for

[15] G. F. Nardelli, in Lectures on Elementary Excitations and Their Interactions in Solids, NATO Advanced Study Institute, Cortina, 1966 (to be published).

[16] G. F. Nardelli, Nuovo Cimento, Suppl. 3, 1124 (1965).

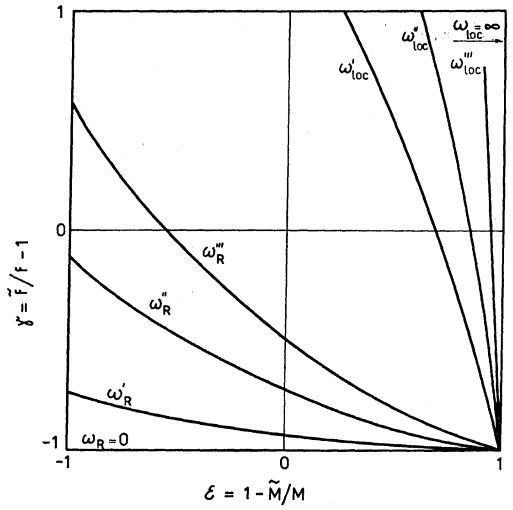

FIG. 2. A qualitative plot of the cosine-mode resonance frequency as a function of the changes of mass, ϵ, and of force constant, $\Delta f/f=\tilde{f}/f-1$, for a diatomic chain or a simple cubic lattice with n.n. interaction.

a defect which affects the mass and the short-range force constants of central type. It appears that the perturbation on the short-range interaction makes $\mathbf{T}$ involve a Γ_1, a Γ_{12}, and, in principle, two Γ_{15} symmetry modes more than does the perturbation on the mass. Indeed, on letting λ go to zero, only a single Γ_{15} symmetry mode

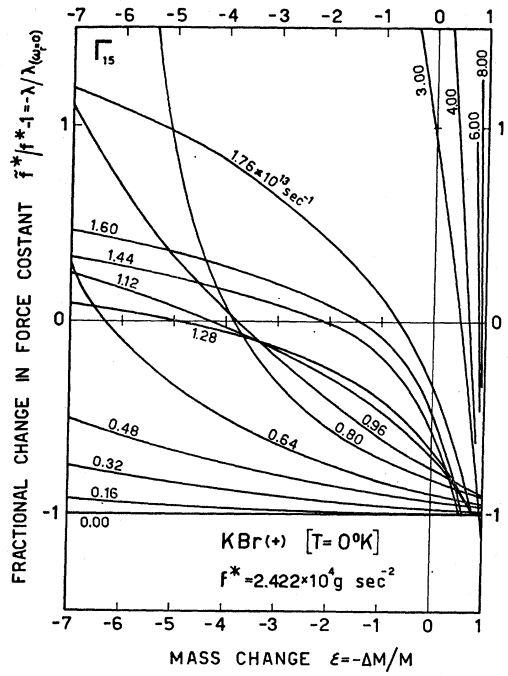

FIG. 3. The Γ_{15} resonance frequency as a function of the changes of mass and effective-force constant for positive defects in KBr at 0°K. The *Reststrahl* and the maximum frequencies are $\omega_T=2.13\times10^{13}$ sec^{-1} and $\omega_{max}=3.15\times10^{13}$ sec^{-1}, respectively. A narrow gap occurs in KBr at $\omega=1.76\times10^{13}$ sec^{-1}.

remains, and $\mathbf{T}$ is seen to approach the usual form for the pure change of mass. The symmetry modes induced in $\mathbf{T}$ by the change in the local interaction do not involve the displacement of the impurity ion. This explains why the Γ_1 and Γ_{12} resonance frequencies do not depend on the change in mass; however, the whole perturbation mixes together the two force-constant-induced Γ_{15} symmetry modes and the mass-induced Γ_{15}, so that a force-constant-induced resonance cannot be separated from the eventual mass-induced resonance in the optical absorption.

Let us now consider the expressions (25). Equations (25a) and (25b) involve only the change of force constant, and for values of $|\lambda|$ not too small, the real parts of $D^{(\Gamma_1)}$ and $D^{(\Gamma_{12})}$ may have some zeros on the frequency axis. Thus, a suitable change of force constant can give rise to resonance modes in which the impurity does not move and the dipole moment is zero for symmetry reasons. These modes do not absorb light, but they can activate a first-order Raman scattering.

With regard to Γ_{15} symmetry modes, by putting $\lambda=0$ it is an easy matter to verify that $D^{(\Gamma_{15})}(z)$ and $\mathbf{N}^{(\Gamma_{15})}(z)$ assume the well-known forms for a pure change of mass; in particular, $\mathbf{N}^{(\Gamma_{15})}(z)$ is seen to become simply $\epsilon\omega^2$, i.e., a real and monotonic function of ω. For $\lambda\neq0$, the matrix $\mathbf{N}^{(\Gamma_{15})}(z)$ is a more complicated function of ω, and it can be responsible for some additional structures in the frequency-dependent absorption coefficient. In our case, it is seen from (25c) that the Γ_{15} resonance condition turns out to be a bilinear form in ϵ and λ, i.e., a hyperbola in the (ϵ,λ) plane, for each value of the resonance frequency ω_R (see Figs. 2 and 3). We have two different sets of hyperbolas, depending on whether the substitutional ion lies on positive or negative lattice sites.

The following consideration seems to be in order at this point. The coefficients of our bilinear form (25c) involve the dynamics of the perfect lattice through the complex-valued BZ integrals $\mathcal{G}_\mu^{\pm}(z)$. It will be shown in Sec. IIB that simplified models, such as the diatomic linear chain, give formally the same result as (25c); however, in crystals having rocksalt structure the BZ integrals $\mathcal{G}_1^{\pm}(z)$, $\mathcal{G}_2^{\pm}(z)$, and $\mathcal{G}_3^{\pm}(z)$ are found to have expressions quite different from the expressions they have in diatomic linear chains. It turns out that expression (25c) actually represents something new with respect to the linear-chain expression. Analogous considerations hold for the linear forms (25a) and (25b).

B. Comparison with the Diatomic Linear Chain

Consider a diatomic linear chain with n.n. interaction; the dispersion relation reads

$$(f-M_{\pm}\omega_{qj}^2)(f-M_{\mp}\omega_{qj}^2)=f^2\cos^2 2\pi r_0 q, \qquad (27)$$

where f is n.n. force constant.

The T matrix for a local change of mass and force constant can be written down straightforwardly; the

resonance denominators turn out to be

$$1+\lambda\chi\mathcal{G}_4^{\pm}(z) \tag{28}$$

for the sine mode, and exactly expression (25c) for the cosine mode. It is understood that BZ integrals $\mathcal{G}_\mu^{\pm}(z)$ ($\mu=1, \cdots, 4$) entering (28) and (25c) are now to be performed in the one-dimensional zone. (28) is seen to be formally equal to the expression for $D^{(\Gamma_1)}$ or $D^{(\Gamma_{12})}$, provided we neglect $\mathcal{G}_5^{\pm}(z)$ in (25a) and (25b), i.e., we neglect the BZ integral which involves different Cartesian components of $\mathbf{e}(\kappa|\mathbf{q}s)$. Furthermore, by keeping in mind that in diatomic linear chains the polarization vectors satisfy the relation

$$e(\pm|qj)/e(\mp|qj)=f\chi^{-1/2}\cos(2\pi r_0 q)/(f-M_{\mp}\omega_{qj}^2), \tag{29}$$

(25c) can be written in a simple form which involves only the $\mathcal{G}_1^{\pm}(z)$ BZ integral. Indeed, from (21), (22), (27), and (29) one can see that $\mathcal{G}_1^{\pm}(z)$, $\mathcal{G}_2^{\pm}(z)$, and $\mathcal{G}_3^{\pm}(z)$ are related to one another by

$$\begin{aligned}\mathcal{G}_2^{\pm}(z)&=[(M_{\pm}M_{\mp})^{1/2}/f]\{(f/M_{\pm}-\omega^2)\mathcal{G}_1^{\pm}(z)-1\},\\ \mathcal{G}_3^{\pm}(z)&=[(M_{\pm}M_{\mp})^{1/2}/f](f/M_{\pm}-\omega^2)\mathcal{G}_2^{\pm}(z),\end{aligned} \tag{30}$$

so that the cosine-mode resonance denominator, the analog of (25c) reads[9] ($\gamma\equiv\lambda M_{\pm}/f$):

$$\begin{aligned}D^{(\cos)}(z)=1+\gamma\{1+(1-\epsilon)M_{\pm}\omega^2/f\}\\ +\{\epsilon(1+\gamma)+\gamma(1-\epsilon)M_{\pm}\omega^2/f\}\omega^2\mathcal{G}_1^{\pm}(z).\end{aligned} \tag{31}$$

At $\lambda=-f/M_{\pm}$, i.e., for the complete decoupling of the impurity from the other particles in the chain, the resonance condition for the cosine mode admits a solution only for $\omega_R=0$, whatever the mass of the impurity. This result is fully consistent with the fact that, in this case, the imperfect chain degenerates into two independent subchains: a linear chain with no cyclic boundary conditions, and a free particle. The resonance at $\omega_R=0$ corresponds to a δ-type peak at zero frequency in the spectral density of the imperfect chain.

By putting $\epsilon=1$, i.e., by considering a defect of vanishing mass, it is an easy matter to verify that at $\lambda=-f/M_{\pm}$ the real parts of $D^{(\cos)}(z)$, the resonance condition for cosine modes, is identically satisfied for all the frequencies. In the (ϵ,λ) plane this corresponds to saying that all the hyperbolas cross the point ($\epsilon=1$, $\lambda=-f/M_{\pm}$) (see Fig. 2).

Let us comment briefly on the essential difference between a linear chain and a crystal lattice with long-range interaction. The essential difference is that in lattices of rocksalt structure with long-range interaction, Eqs. (30) are no longer expected to hold, so that the hyperbolas which correspond to the same kind of symmetry do not cross the same point in the (ϵ,λ) plane.

In the ionic type of lattice, every ion interacts with its neighbors essentially through hard-core (overlap), Coulomb, and dipolar forces.[17] Also, when the overlap interaction is completely removed, the motion of a foreign ion is always coupled with the vibrating surrounding ions by Coulomb and dipolar forces. Such a physical situation is responsible for two kinds of effects: (i) the value λ_0 which accounts for the resonance at $\omega_R=0$ does not correspond to the vanishing of the overlap interaction, because Coulomb and dipolar forces contribute to the n.n. force constant through a term which makes the hard-core repulsion softer[12,17]; (ii) when we let ϵ go to zero with a fixed resonance frequency $\omega_R>0$, the value of λ which accounts for the resonance at this frequency does not approach λ_0, because Coulomb and dipolar coupling for a vibrating charged particle differs from the coupling of the particle at rest.

Property (ii) corresponds to saying that on letting ω_R go to zero and ϵ to unity, the hyperbolas will thicken up in the neighborhood of the straight line $\lambda=\lambda_0$, but they no longer cross the point ($\epsilon=1$, $\lambda=\lambda_0$). The actual situation is shown in Fig. 3. It appears that the value of λ_0 does not correspond to $-f/M(\pm)$, i.e., to the vanishing of the bare hard-core repulsion. This fact suggests a way to define an "effective" force constant f^*.

III. THE EFFECTIVE FORCE CONSTANT

Let f^* denote the effective n.n. force constant of central type in a rocksalt-type lattice. In the present approach it represents the combined effects of hard-core, Coulomb, and dipolar forces. A way to obtain a definition of f^* is suggested by the result [see expression (31)] for the linear chain with n.n. interaction. Indeed, requiring (25c) to have a resonance at $\omega_R=0$ enables us to define f^* by the BZ integral:

$$\begin{aligned}f^*=-M(\pm)\lambda_0=\Big\{v\sum_{s=1}^{6}\int_{\mathrm{BZ}}d\mathbf{q}\omega_{\mathbf{q}s}^{-2}\\ \times[M^{-1/2}(\pm)e_x(\pm|\mathbf{q}s)-M^{-1/2}(\mp)e_x(\mp|\mathbf{q}s)\\ \times\cos 2\pi r_0 q_x]^2\Big\}^{-1}.\end{aligned} \tag{32}$$

For a lattice with long-range interaction, expression (32) can not be easily explicated with respect to physical quantities, such as compressibility, electronic polarizabilities $\alpha_{\pm}$, and effective charge e^*, which usually enter the definition of the dynamical matrix. Then, the use of (32) requires the knowledge of all the frequencies $\omega_{\mathbf{q}s}$ and polarization vectors $\mathbf{e}(\kappa|\mathbf{q}s)$ of the perfect lattice. In the definition of f^*, as given by (32), a defect has been used as the external probe to sample the short-range interaction in our lattice. Of course, (32) represents the low-frequency effective-force constant.

In order to allow for an estimation of f^* in terms of the physical quantities we have mentioned above, we try to introduce the effective-force constant starting from a different point of view. In Hardy's deformation-

[17] J. R. Hardy, Phil. Mag. 7, 315 (1961).

dipole (DD) model[17] the force-constant matrix reads

$$\mathbf{\Phi}^{(DD)}=\mathbf{\Phi}^{(R)}+(1+\mathbf{S}\mathbf{e}^{-1})\mathbf{\Phi}^{(C)} \times(1-\mathbf{e}^{-1}\boldsymbol{\alpha}\mathbf{e}^{-1}\mathbf{\Phi}^{(C)})^{-1}(1+\mathbf{e}^{-1}\mathbf{S}^{T}), \quad (33)$$

where $\mathbf{\Phi}^{(R)}$ is the rigid-ion hard-core contribution, $\mathbf{\Phi}^{(C)}$ is the matrix for the Coulomb interaction, $\mathbf{e}$ is the matrix of the bare ionic charges, and $\boldsymbol{\alpha}$ the matrix of the electronic polarizability of the ions. The matrix $\mathbf{S}$ ($\mathbf{S}^T$ denotes the transposed matrix) is defined in Hardy's[17] paper; in (33) it represents the correction due to the dipole moment which is induced by the ion deformation, i.e., the correction due to the transfer of electric charge. Notice that matrix $\mathbf{S}$ involves Szigeti's effective charge e_S^* ($\mathbf{S}=0$ means $e_S^*=e$). It appears from (33) that a nonvanishing polarizability of the ions gives rise to terms with increasing powers of $\mathbf{\Phi}^{(C)}$ (dipole, quadrupole, etc., interactions); furthermore the matrix $\mathbf{S}$ is responsible for a weakening in the rigid-ion hard-core interaction. In the neighborhood of the zone center it is a simple matter to verify that expression (33) admits the following decomposition:

$$\mathbf{\Phi}^{(DD)}=\mathbf{\Phi}_{\rm eff}{}^{(R)}+\mathbf{\Phi}_{\rm eff}{}^{(C)}, \quad (\mathbf{q}\approx 0), \quad (34)$$

where $\mathbf{\Phi}_{\rm eff}{}^{(R)}$ and $\mathbf{\Phi}_{\rm eff}{}^{(C)}$ are the usual matrices for hard-core and Coulomb interaction with f and e simply replaced by f^* and e^*, respectively. e^* is equal to the Szigeti effective charge e_S^*,[18] while, neglecting the deformation of the positive ion, the value of f^* turns out to be

$$f^*=\frac{e^2}{v}\left\{A+2B-\frac{8\pi}{3}\left(\frac{e_S^*}{e}\right)^2\frac{\alpha_++\alpha_-}{\alpha_++\alpha_-+3v/8\pi}\right\}. \quad (35)$$

In writing (35) we have employed the usual notation

$$A=(2v/e^2)[d^2\varphi^{(R)}(r)/dr^2]_{r=r_0},$$
$$B=(2v/e^2)[d\varphi^{(R)}(r)/rdr]_{r=r_0},$$

for central and noncentral force constants due to the hard-core interaction. On the assumption that the decomposition (34) holds for practical purposes with the same choice for f^* and e^* in all the points of the BZ expression (35) is expected to yield the same result as expression (32). Table I shows the comparison between the values of f^* as evaluated from (32) and (35). From the above considerations it follows that f^*, as given by (35), is just a sort of center-of-zone effective-force constant.

TABLE I. Comparison between n.n. hard-core force constants for rigid-ion model (1st column), effective n.n. force constants in DD model (2nd column), and effective n.n. force constants deduced from fitting vanishing Γ_{15} resonance frequency.

Crystal	$A+2B$	$(v/e^2)f^{*a}$	$(v/-e^2)M(\pm)\lambda_0{}^b$
NaCl	7.98	6.15	5.95
KCl	9.36	7.55	7.20
KBr	9.62	7.73	7.58
KI	10.01	8.32	8.16

[a] Equation 35.
[b] Equation 32.

[18] E. Burstein, in *Proceedings of the International Conference on Lattice Dynamics, Copenhagen, 1963*, edited by R. F. Wallis (Pergamon Press, Inc., New York, 1965), p. 315.

IV. THE RESPONSE FUNCTIONS

We are concerned with the effect of defects on two typical response functions, namely, the dielectric susceptibility tensor $\boldsymbol{\chi}(\mathbf{k},\omega)$ and the thermal conductivity tensor $\boldsymbol{\kappa}(\mathbf{k},\omega)$. Usually the evaluation of these response functions is approached by the simplifying assumptions of the electric-dipole approximation in the photon-phonon interaction and the relaxation-time approximation in the phonon-transport equation.

Our purpose here is to show that both dielectric susceptibility and thermal conductivity can be expressed in terms of the irreducible T matrix we have introduced in Sec. II.

A. The Dielectric Susceptibility Tensor

The Kubo expression for the dielectric susceptibility tensor reads[19]

$$\chi_{\mu\nu}(\mathbf{k},\omega)=V^{-1}\int_0^\infty dt e^{-i(\omega-i0^+)t} \times\int_0^\beta d\beta'\langle\mathfrak{M}_\nu'(-\mathbf{k},-i\hbar\beta')\mathfrak{M}_\mu(\mathbf{k},t)\rangle, \quad (36)$$

where $\mathbf{k}$ and ω are the photon wave vector and frequency, V is the crystal volume, and $\beta=1/k_BT$ (k_B = Boltzmann constant, T = absolute temperature). The indices μ and ν denote Cartesian components with respect to the intrinsic frame $\mathbf{i}_\mu(\mu=1,2,3)$ of the photon, i.e., the frame in which the $\mathbf{i}_3$ axis is oriented in the same direction as $\mathbf{k}$. The operator $\mathfrak{M}(\mathbf{k})$ is the Fourier transform of the dipole-moment operator of our crystal. Since we are interested in the infrared (IR) region, $\mathfrak{M}(\mathbf{k})$ turns out to be

$$\mathfrak{M}(\mathbf{k})=\textstyle\sum_l e^{i\mathbf{k}\cdot\mathbf{x}_l}e(l)\mathbf{u}(l), \quad (37)$$

where $\mathbf{x}_l$ is the lattice vector (here l represents both Bravais and cell indices $\mathbf{l}$ and κ), $e(l)$ the electric charge, and $\mathbf{u}(l)$ is the displacement of the lth ion.

In expression (36) we have put

$$\mathfrak{M}(\mathbf{k},s)\equiv e^{isH/\hbar}\mathfrak{M}(\mathbf{k})e^{-isH/\hbar} \quad (38)$$

and

$$\mathfrak{M}'(\mathbf{k},s)\equiv-(i/\hbar)[\mathfrak{M}(\mathbf{k},s),H] \quad (39)$$

for either $s=t$ or $s=-i\hbar\beta'$. H is the crystal Hamiltonian, and the brackets $\langle\cdots\rangle$ denote ensemble average at thermal equilibrium. In the IR region, the dielectric susceptibility tensor is simply related to the dynamical matrix of our crystal, regardless of the degree of perfec-

[19] A. A. Maradudin, Phys. Rev. 123, 777 (1961).

tion of the crystal itself. In order to see this, we expand $\mathfrak{M}(\mathbf{k}s)$ as

$$\mathfrak{M}(\mathbf{k},s)=\sum_\lambda \sum_l e^{-i\mathbf{k}\cdot\mathbf{x}_l} e(l) \times(\hbar/2M(l)\omega_\lambda)^{1/2}\psi_\lambda'(l)(b_\lambda(s)+b_{-\lambda}^\dagger(s)). \quad (40)$$

Here b_λ and $b_\lambda^\dagger$ denote phonon destruction and creation operators, respectively, for the perturbed modes of the lattice. $M(l)$ is the mass of the ion at the lth lattice site. In writing the expression (40) we have used the conventions

$$\psi_{-\lambda}'(l)=\psi_\lambda'^*(l); \quad \omega_{-\lambda}=\omega_\lambda.$$

If we keep in mind that

$$b_\lambda(s)=b_\lambda(0)e^{-i\omega_\lambda s}; \quad b_\lambda^\dagger(s)=b_\lambda^\dagger(0)e^{i\omega_\lambda s}, \quad (41)$$

substitution of expression (40) in the integrand of (36) gives

$$\langle\mathfrak{M}_\nu'(-\mathbf{k},-i\hbar\beta')\mathfrak{M}_\mu(\mathbf{k},t)\rangle=\tfrac{1}{2}\hbar\langle\sum_\lambda\sum_{ll'} \times e^{-i\mathbf{k}\cdot(\mathbf{x}_l-\mathbf{x}_{l'})}e(l)e(l')M^{-1/2}(l) \times M^{-1/2}(l')\mathbf{i}_\nu\cdot\psi_\lambda'(l)\psi_\lambda'^*(l')\cdot\mathbf{i}_\mu \times\{\langle n_\lambda\rangle_\beta e^{-i\omega_\lambda t+\omega_\lambda\hbar\beta'}-\langle n_\lambda+1\rangle_\beta e^{i\omega_\lambda t-\omega_\lambda\hbar\beta'}\}\rangle_{\mathrm{av}}, \quad (42)$$

where n_λ denotes phonon occupation-number operator. The ensemble average has been split into the statistical average over all the possible configurations of defects, here denoted by $\langle\cdots\rangle_{\mathrm{av}}$ and the thermal average $\langle\cdots\rangle_\beta$ over the canonical distribution of phonons for a given configuration of defects.

By taking into account that

$$\langle n_\lambda\rangle_\beta=(e^{\beta\hbar\omega_\lambda}-1)^{-1}, \quad (43)$$

the integrations on β' and t which appear in expression (36) can be easily performed; one obtains

$$\chi_{\mu\nu}(\mathbf{k},\omega)=V^{-1}\langle\sum_\lambda(-\mathbf{k},\nu|\,\mathbf{e}\mathbf{M}^{-1/2}|\psi_\lambda') \times(\omega_\lambda^2-\omega^2-2i\omega 0^+)^{-1}(\psi_\lambda'|\mathbf{M}^{-1/2}\mathbf{e}|\,\mu,-\mathbf{k})\rangle_{\mathrm{av}}. \quad (44)$$

Here $\mathbf{e}$ denotes electric charge matrix.

In writing the expression (44) we have considered the linear vector space defined by the complete set of normal modes ψ_λ'. The symbols $|\psi_\lambda')$ and $|\nu,\mathbf{k})$ denote vectors in this space and the scalar product is defined by

$$(\mathbf{k},\nu|\psi_\lambda')\equiv\sum_l e^{-i\mathbf{k}\cdot\mathbf{x}_l}\mathbf{i}_\nu\cdot\psi_\lambda'(l). \quad (45)$$

Equation (44) exhibits the spectral representation of $(\mathbf{L}_A-\omega^2-2i\omega 0^+)^{-1}$. Thus we can write:

$$\chi_{\mu\nu}(\mathbf{k},\omega)=V^{-1}\langle(-\mathbf{k},\nu|\,\mathbf{e}\mathbf{M}_A^{-1/2}(\mathbf{L}_A-z)^{-1} \times\mathbf{M}_A^{-1/2}\mathbf{e}|\,\mu,-\mathbf{k})\rangle_{\mathrm{av}}. \quad (46)$$

Notice that the explicit dependence of $\chi_{\mu\nu}$ on temperature has disappeared.

Consider now a cubic lattice with two atoms per unit cell and let $|\mathbf{q},s)$ be the unperturbed lattice wave in the linear vector space defined above:

$$(\mathbf{l},\kappa|\mathbf{q},s)=N^{-1/2}\mathbf{e}(\kappa|\mathbf{q},s)e^{i\mathbf{q}\cdot\mathbf{x}(\mathbf{l},\kappa)}. \quad (47)$$

Here $\mathbf{e}(\kappa|\mathbf{q},s)$ is the polarization vector of the sth branch and N is the number of primitive cells of our crystal.

With the help of the completeness relation

$$\sum_{\mathbf{q},s}|\mathbf{q},s)(s,\mathbf{q}|=\mathbf{I}, \quad (48)$$

the use of (4) and (16) in (46) gives

$$\chi_{\mu\nu}(\mathbf{k},\omega)=V^{-1}\sum_{ss'}\sum_{\mathbf{q}}(-\mathbf{k},\nu|\,\mathbf{e}\mathbf{M}_0^{-1/2}|\,s,-\mathbf{q}) \times(-\mathbf{q},s|\,(\mathbf{L}_0+p\mathbf{T}(z)-z)^{-1}|\,s',-\mathbf{q}) \times(-\mathbf{q},s'|\mathbf{M}_0^{-1/2}\mathbf{e}|\,\mu,-\mathbf{k}). \quad (49)$$

Here $\mathbf{T}(z)$ is the matrix we have defined by (14). Keeping in mind the above definition of scalar product, we have

$$(\mathbf{k},\nu|\,\mathbf{e}\mathbf{M}_0^{-1/2}|\,s,\mathbf{q})=N^{-1/2}\delta_{\mathbf{q},\mathbf{k}} \times\sum_\kappa e(\kappa)\mathbf{M}_0^{-1/2}(\kappa)e_\nu(\kappa|\mathbf{k},s), \quad (50)$$

where $\delta_{\mathbf{q},\mathbf{k}}$ accounts for the wave-vector conservation. Since the photon wave vector $\mathbf{k}$ has negligible magnitude on the phonon scale, the phonon involved in (50) practically lies at the center of the BZ. Furthermore, expression (50) vanishes when s refers to acoustic branches. Then s ($s=1, 2, 3$) can be considered to label only the three optic branches. With no loss of generality we can assume that s and ν label the same axes, so at $\mathbf{q}\approx 0$ we have $|e_\nu(\kappa|0,s)|=|e_\nu(\kappa|0,\nu)|\,\delta_{\nu s}$. Thus the phonon involved in (50) is seen to have the same type of polarization as the photon, and expression (49) can be written as

$$\chi_{\mu\nu}(\omega)=(e^{*2}/\mu v)(\mathbf{q}\approx 0,\nu|\,[\mathbf{L}_0+p\mathbf{T}(z)-z]^{-1}|\,\mu,\mathbf{q}\approx 0). \quad (51)$$

Here e^* is the macroscopic effective charge associated with the $\mathbf{q}\approx 0$ optic mode,[18] $\mu=M(\pm)M(\mp)/[M(\pm)+M(\mp)]$ is the reduced mass, and $v=V/N$ the volume of the primitive cell.

In the wave-vector representation, $\mathbf{L}_0+p\mathbf{T}(z)-z$ is a 6×6 matrix. We label rows and columns by the double index (ν,r): by $\nu=1, 2$ we denote transverse and by $\nu=3$ longitudinal waves, while by $r=A,O$ we denote acoustic or optic waves, respectively. Consider the 6×6 linear vector space defined by the complete set of 6-row polarization vectors $e(\mathbf{q},\nu,r)$; the inversion of our 6×6 matrix can be made easy by considering the irr.rep. of the group of wave vector $\mathbf{q}$. At the center of the zone, both acoustic $e(0,\nu,A)$ and optic $e(0,\nu,O)$ 6-row polarization vectors in the NaCl-type of lattice transform according to the Γ_{15} irr.rep.; we identify these 6-row vectors by $|r,\nu)$ ($r=A, O$; $\nu=1, 2, 3$). On the right-hand side of (51) there appears the matrix element

$$(\nu,O|\,[\mathbf{L}_0+p\mathbf{T}(z)-z]^{-1}|\,O,\mu). \quad (52)$$

From Schur's lemma,

$$(\nu,r|\,\mathbf{T}(z)\,|r',\mu)=\delta_{\nu\mu}T_{rr'}(z), \quad (53)$$

it follows that expression (52) is diagonal with respect

to μ and ν indices. Thus, we have to perform the inversion of the 2×2 matrix

$$\begin{pmatrix} -z+pT_{AA}(z) & pT_{AO}(z) \\ pT_{OA}(z) & \omega_T{}^2-z+pT_{OO}(z) \end{pmatrix} \tag{54}$$

for both $\mu=1$ and $\mu=2$, i.e., for transverse waves, and of an analogous matrix with ω_T replaced by ω_L for longitudinal waves, i.e., $\mu=3$. Here ω_T and ω_L are, respectively, the transverse and longitudinal optic frequencies at $\mathbf{q}=0$, and T_{AA}, T_{OO} and $T_{AO}=T_{OA}$ are the matrix elements of the projected $\mathbf{T}(z)$ into our 6×6 subspace. The projection of $\mathbf{T}(z)$ can be easily performed by means of the following transformation coefficients:

$$\begin{aligned} &(\nu,r|\,\Gamma_{15},\ j=1,\ \mu)=\delta_{\mu\nu}e_\nu(\pm|\,\mathbf{q}=0,\ r,\ \nu)\,,\\ &(\nu,r|\,\Gamma_{15},\ j=2,\ \mu)=2^{1/2}\delta_{\mu\nu}e_\nu(\mp|\,\mathbf{q}=0,\ r,\ \nu)\,,\\ &(\nu,r|\,\Gamma_{15},\ j=3,\ \mu)=2\delta_{\mu\nu}e_\nu(\mp|\,\mathbf{q}=0,\ r,\ \nu)\,. \end{aligned} \tag{55}$$

In writing (55) the Γ_{15} symmetry vectors in the subspace of the perturbation have been considered in full: index $\mu=x,\ y,\ z$ labels the rows of the irr. rep., while j retains the same meaning as in Sec. II. T_{AA}, T_{OO}, and T_{AO} are found to be

$$T_{OO}(z)=\frac{1}{(1+\chi)D^{(\Gamma_{15})}(z)}\{N_{11}{}^{(\Gamma_{15})}+2\chi N_{22}{}^{(\Gamma_{15})}-2^{3/2}\chi^{1/2}N_{12}{}^{(\Gamma_{15})}\}\,, \tag{56a}$$

$$T_{AA}(z)=\frac{1}{(1+\chi)D^{(\Gamma_{15})}(z)}\{\chi N_{11}{}^{(\Gamma_{15})}+2N_{22}{}^{(\Gamma_{15})}+2^{3/2}\chi^{1/2}N_{12}{}^{(\Gamma_{15})}\}\,, \tag{56b}$$

$$T_{AO}(z)=T_{OA}(z)=\frac{1}{(1+\chi)D^{(\Gamma_{15})}(z)}\{\chi^{1/2}N_{11}{}^{(\Gamma_{15})}-2\chi^{1/2}N_{22}{}^{(\Gamma_{15})}+2^{1/2}(1-\chi)N_{12}{}^{(\Gamma_{15})}\}\,, \tag{56c}$$

where $N_{11}{}^{(\Gamma_{15})}$, $N_{22}{}^{(\Gamma_{15})}$ and $N_{12}{}^{(\Gamma_{15})}=N_{21}{}^{(\Gamma_{15})}$ are the matrix elements of $\mathbf{N}^{(\Gamma_{15})}(z)$ in (24c). Thus $\chi_{11}(\omega)=\chi_{22}(\omega)=\chi_T(\omega)$ and $\chi_{33}(\omega)=\chi_L(\omega)$ are recognized to be the transverse and longitudinal dielectric susceptibilities, respectively. $\chi_T(\omega)$ turns out to be

$$\chi_T(\omega)=(e^{*2}/\mu v)\{\omega_T{}^2-z+pT_{OO}(z)+p^2T_{AO}{}^2(z)/(z-pT_{AA}(z))\}^{-1}\,, \tag{57}$$

where $z=\omega^2+2i\omega0^+$. An analogous expression holds for $\chi_L(\omega)$. In deriving expression (57) no assumptions have been made other than the hypothesis of pure random distribution of defects and negligible contribution to $\mathbf{T}_{A,\mathrm{irr}}$ by irreducible graphs involving different scattering centers. In (57), multiple scattering by different defects is considered through reducible graphs only. The latter rather than the former assumption makes it doubtful whether Eq. (57) is also reliable in the high- or intermediate-concentration case.

T_{AO} and T_{AA} enter the denominator of (57) with the second and third or higher powers of p, respectively. This is accounted for by looking at the reducible graphs; the smallest order reducible graphs involving T_{AO} and T_{AA} are shown in Fig. 4. Hereafter we consider the low-concentration limit.

Assume first that ω belongs to the vibrational continuum; then by disregarding the last term in the denominator of (57), and using Eqs. (23) and (24c), the complex dielectric susceptibility reads

$$\begin{aligned} \chi_T{}^{(1)}(\omega)&=\frac{e^{*2}}{\mu v}\frac{\omega_T{}^2+p\ \mathrm{Re}T_{OO}(\omega^2+i0^+)-\omega^2}{[\omega_T{}^2+p\ \mathrm{Re}T_{OO}(\omega^2+i0^+)-\omega^2]^2+[p\ \mathrm{Im}T_{OO}(\omega^2+i0^+)]^2}\\ &=\frac{e^{*2}}{\mu v}\frac{(\omega_T{}^2-\omega^2)(D_1{}^2+D_2{}^2)+p(N_1D_1+N_2D_2)}{[(\omega_T{}^2-\omega^2)D_1+pN_1]^2+[(\omega_T{}^2-\omega^2)D_2+pN_2]^2}\,, \end{aligned} \tag{58a}$$

$$\begin{aligned} \chi_T{}^{(2)}(\omega)&=\frac{e^{*2}}{\mu v}\frac{-p\ \mathrm{Im}T_{OO}(\omega^2+i0^+)}{[\omega_T{}^2+p\ \mathrm{Re}T_{OO}(\omega^2+i0^+)-\omega^2]^2+[p\ \mathrm{Im}T_{OO}(\omega^2+i0^+)]^2}\\ &=\frac{e^{*2}}{\mu v}p\frac{D_2N_1-D_1N_2}{[(\omega_T{}^2-\omega^2)D_1+pN_1]^2+[(\omega_T{}^2-\omega^2)D_2+pN_2]^2}\,, \end{aligned} \tag{58b}$$

where we have put $T_{OO}(z)=(N_1+iN_2)/(D_1+iD_2)$ and $\chi_T=\chi_T{}^{(1)}+i\chi_T{}^{(2)}$.

Consider now a frequency outside the vibrational continuum; in this case the complex susceptibility is found

to be

$$\chi_T^{(1)}(\omega)=\frac{e^{*2}}{\mu v}\mathcal{P}\frac{D_1}{(\omega_T^2-\omega^2)D_1+pN_1}=\frac{e^{*2}}{\mu v}\left\{\frac{1}{\omega_T^2-\omega^2}-\frac{pN_1}{\omega_T^2-\omega^2}\mathcal{P}\frac{1}{(\omega_T^2-\omega^2)D_1+pN_1}\right\}, \tag{59a}$$

$$\chi_T^{(2)}(\omega)=\frac{e^{*2}}{\mu v}\frac{p\pi N_1}{\omega_T^2-\omega^2}\delta\{(\omega_T^2-\omega^2)D_1+pN_1\}. \tag{59b}$$

In Eq. (59), $\mathcal{P}$ and $\delta\{\cdots\}$ denote Cauchy principal value and δ function, respectively. The absorption coefficient for electromagnetic radiation is defined by

$$\alpha_T(\omega)=(4\pi\omega/\eta c)\chi_T^{(2)}(\omega), \tag{60}$$

where η is the refractive index and c is velocity of light. For a frequency in the vibrational continuum $\alpha_T(\omega)$ is seen to be

$$\alpha_T(\omega)=\frac{4\pi e^{*2}}{\mu v\eta c}\frac{\omega}{(\omega_T^2-\omega^2)^2}\frac{p(D_2N_1-D_2N_2)}{[D_1+p(\omega_T^2-\omega^2)^{-1}N_1]^2+[D_2+p(\omega_T^2-\omega^2)^{-1}N_2]^2}, \tag{61}$$

as follows from (58b).

Equation (61) exhibits the resonance denominator for optical absorption at the vibrational continuum. On the basis of the above expressions it is an easy matter to analyze the peculiarities that the absorption coefficient of an imperfect ionic lattice exhibits in the whole IR frequency range. The defects produce three types of effects: (i) in the frequency region near ω_T they have the effect of replacing the δ peak at the *Reststrahlen* frequency by the Lorentzian-shaped expression (61) which is peaked at the shifted frequency $\omega_T^2+p\times\mathrm{Re}T_{OO}(\omega_T^2+i0^+)$; (ii) in the region outside the vibrational continuum they give rise to δ peaks at about the local- and gap-mode frequencies, and (iii) they make the crystal lattice able to absorb light at any frequency of the vibrational continuum, with Lorentzian-shaped peaks at about the resonance frequencies. The last two effects appear clearly by considering the expression (56a) for the optic-active element of the scattering matrix. Indeed, the frequencies for which the real part $D_1(\omega^2)$ of the denominator vanishes correspond either to resonance scattering or to local and gap modes, whether ω is or is not a frequency of the vibrational continuum.[14] Equation (59b) makes statement (ii) obvious. As regards statement (iii), let us assume that a root (say ω_R) of the equation

$$D_1(\omega^2)=0 \tag{62}$$

exists inside the vibrational continuum. It appears from (61) that $\alpha_T(\omega)$ exhibits a Lorentzian-shaped peak at the shifted frequency

$$\tilde{\omega}_R^2\cong\omega_R^2-pN_1(\omega_R^2)/(\omega_T^2-\omega_R^2)D_1'(\omega_R^2). \tag{63}$$

By a prime on D_1 we have denoted the derivative with respect to ω^2. This peak is called "resonance absorption." Notice that broader peaks may occur when the resonance condition (62) is approximatively satisfied. In the neighborhood of the peak frequency, the absorption coefficient can be written as

$$\alpha_T(\omega)\cong\frac{4\pi e^{*2}\omega}{\mu v\eta c}pf(\tilde{\omega}_R^2)\frac{\Gamma(\tilde{\omega}_R^2)}{(\omega^2-\tilde{\omega}_R^2)^2+\Gamma^2(\tilde{\omega}_R^2)}, \tag{63a}$$

where $f(\tilde{\omega}_R^2)$, the strength factor, is given by

$$f(\tilde{\omega}_R^2)=\frac{1}{\omega_T^2-\omega_R^2}\frac{N_1(\tilde{\omega}_R^2)}{(\omega_T^2-\tilde{\omega}_R^2)D_1'(\tilde{\omega}_R^2)+pN_1'(\tilde{\omega}_R^2)}, \tag{64}$$

and the width is given by

$$\Gamma(\tilde{\omega}_R^2)=\frac{D_2(\tilde{\omega}_R^2)+p(\omega_T^2-\tilde{\omega}_R^2)^{-1}N_2(\tilde{\omega}_R^2)}{D_1'(\tilde{\omega}_R^2)+p(\omega_T^2-\tilde{\omega}_R^2)^{-1}N_1'(\tilde{\omega}_R^2)}\cong\Gamma_0+p\Gamma_1. \tag{65}$$

$\Gamma_0=D_2/D_1'$ is seen to be the proper width of the resonance, i.e., the width coming from the scattering due to the defect itself;

$$\Gamma_1=(N_1'D_2-N_2D_1')/(\omega_T^2-\tilde{\omega}_R^2)D_1'^2 \tag{66}$$

represents the additional width which is due to the reducible-graph multiple scattering by different defects.

B. The Thermal Conductivity Tensor

We conclude this section with some remarks on the thermal conductivity. In the relaxation-time approxi-

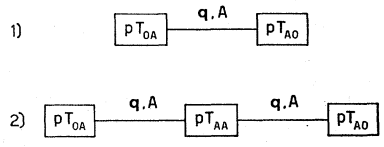

FIG. 4. Smallest order reducible graphs involving $T_{AO}(z)=T_{OA}(z)$ (1) and $T_{AA}(z)$ (2).

mation, the thermal conductivity tensor reads[20]

$$\kappa(\omega,\mathbf{k})=\int dq\, C_q \frac{v_G(q)v_G(q)}{\tau_q^{-1}+i(\omega-\mathbf{k}\cdot\mathbf{v}_G)}, \quad (67)$$

where C_q is the heat capacity of phonons of wave vector $\mathbf{q}$ and polarization s, $v_G(q)$ is the group velocity, and τ_q is the relaxation time. Under the action of an external temperature gradient the quantity which is actually measured is $\kappa=\kappa(0,0)$, namely, expression (67) for ω and $\mathbf{k}$ equal to zero. All the processes which affect the free-phonon propagation in crystals contribute to τ_q^{-1}, and it is usually assumed that they contribute independently. It has been recently pointed out by Klein[21] that to lowest order in the concentration of defects the inverse of the relaxation time, as limited by the defect phonon scattering, is essentially just the imaginary part of the matrix element of $\mathbf{T}(z)$ with respect to the free normal mode of wave vector $\mathbf{q}$ and polarization s, i.e.,

$$(\tau_{\mathbf{q},s}^{-1})_{\text{defects}}=-p\pi\omega_{\mathbf{q},s}^{-1} \times \mathrm{Im}\langle \mathbf{q},s|\mathbf{T}(\omega^2+i0^+)|s,\mathbf{q}\rangle. \quad (68)$$

In the above expression, p is the fractional concentration of defects. It is worth while to note that the relaxation time involves all the irr.rep. which appear in the T matrix, so that it would be one of the most interesting quantities to measure experimentally; unfortunately, κ is an integral functional of the phonon distribution, and a large part of the sensitivity of τ_q with respect to the phonon scattering is lost in performing the integral over q space.

A good sensitivity is retained at very low temperatures, but there the defect contribution to the thermal conductivity is expected to be dominated by resonance scattering of Γ_{15} symmetry, the same symmetry involved in the absorption coefficient. The phonon heat capacity is indeed significantly different from zero for $\hbar\omega_q \lesssim k_B T$, and we could show easily that the symmetry modes of T which have nonvanishing projection on the free acoustic modes at the zone center (i.e., at $\mathbf{q}\approx 0$) are just the Γ_{15} symmetry modes. We conclude that we can hope to draw more physical information from thermal conductivity measurements than from optical measurements only when unusual accuracy is obtained in performing the experiments.

V. NUMERICAL RESULTS AND DISCUSSION

A. Results for the Absorption Coefficient

We have performed numerical calculations for several rocksalt-type lattices: Hardy's DD model and zero-temperature crystal data were used for the host-lattice dynamics.[17,22]

To evaluate the complex-valued integrals $\mathcal{G}_\mu^{\pm}(z)$ a grid of 4096 points in the Brillouin zone was chosen. Here we restrict ourselves to reporting, as an example, the numerical results for KBr crystals containing positive defects. The results for several other crystals (but not KI, for which see Ref. 12) will be presented in a subsequent paper. Figure 3 shows the hyperbolas in the (ϵ,λ) plane corresponding to different Γ_{15} resonance frequencies. Instead of λ we report the fractional change of effective force constant, i.e., $\tilde{f}^*/f^*-1$, with f^* given by Eq. (35). In the low- or high-frequency limit the hyperbolas approach a horizontal or a vertical straight line, respectively. In both cases the hyperbolas become very close to one another: The frequencies of low-lying resonance modes are seen to depend critically on the change in force constant and to be quite insensitive to the change in mass. The reverse holds for the frequency of strongly localized modes. Indeed, in the theory of strongly localized modes (as for the U center) the change in force constant enters as a correction,[11] while it accounts by itself for the existence of a low-frequency resonance, when the impurity is weakly bound to its neighbors ($\tilde{f}^*\to 0$). These circumstances also explain some striking effects induced in resonance modes[23,24] by a lattice strain. It is instructive to plot the change in force constant versus the resonance frequency for different

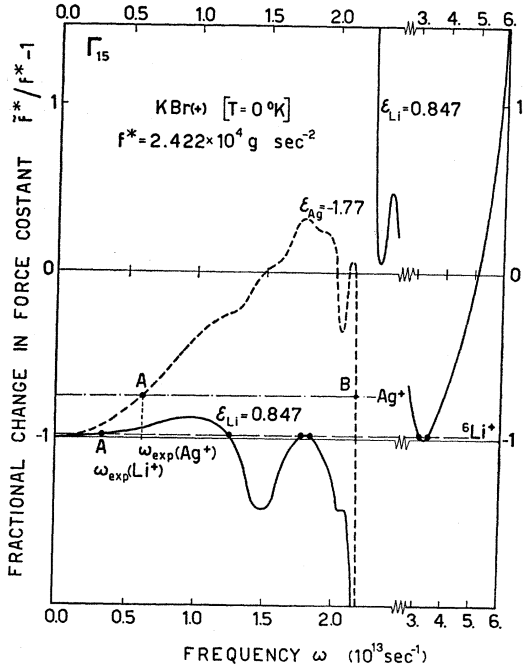

FIG. 5. Plots of the change in force constant versus resonance frequency of Γ_{15} modes for two different impurity masses: Li^+ ($\epsilon=0.847$) and Ag^+ ($\epsilon=-1.77$). Points A refer to experimental peak frequencies.

[20] P. Carruthers, Rev. Mod. Phys. 33, 92 (1961).
[21] M. V. Klein, Phys. Rev. 141, A716 (1966).
[22] A. M. Karo and J. R. Hardy, Phys. Rev. 129, 2024 (1963).
[23] G. Benedek and G. F. Nardelli, Phys. Rev. Letters 16, 517 (1966).
[24] I. G. Nolt and A. J. Sievers, Phys. Rev. Letters 16, 1103 (1966).

values of ϵ. Figure 5 shows this plot for two weakly coupled ions in KBr, i.e., $^6Li^+$ ($\epsilon=0.847$) and Ag^+ ($\epsilon=-1.77$). The intersections with the horizontal axis (i.e., $\lambda=0$) give the pure-change-of-mass predictions for the resonance absorption. It is well known[2,9] that both $^6Li^+$ and Ag^+ as impurities in KBr are able to induce a very strong and narrow resonance at low frequencies and a broad absorption band at somewhat higher frequencies. The oscillator strength for the broad band is much larger for Ag^+ than for Li^+. In Fig. 4 the abscissa of the point A corresponds to the experimental frequency of the resonance absorption. From the ordinate one obtains the value of the effective coupling between the impurity and its n.n. According to our model one

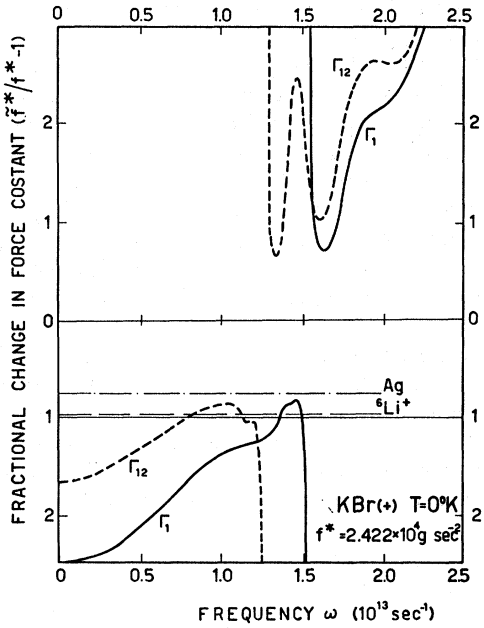

FIG. 6. Plots of the change in force constant versus resonance frequency of Γ_1 and Γ_{12} modes. The effective-force constant change fitted to the experimental IR absorption peak is reported for $^6Li^+$ and Ag^+.

obtains:

$$\tilde{f}^*(^6Li^+)=0.015f^*, \tag{69a}$$

$$\tilde{f}^*(Ag^+)=0.23f^*. \tag{69b}$$

Note that for KBr:$^6Li^+$ a resonance at $\omega=1.24\times10^{13}$ sec^{-1} and two other resonances at $\omega=1.80\times10^{13}$ sec^{-1} very close to one another are also predicted. These are expected to be very broad, since the projected density of states is quite large at such frequencies. Beyond this, a localized doublet not too far from the maximum frequency $\omega_{max}=3.10\times10^{13}$ sec^{-1} should exist also. For KBr:Ag^+ no other resonance is expected from the fitted value (69b) of $\tilde{f}^*$, except for the resonance at the point B in Fig. 5, which occurs too close to the *Reststrahlen* frequency ever to be detected. Figure 6 shows the resonance condition for Γ_1 or Γ_{12} symmetry modes. Since

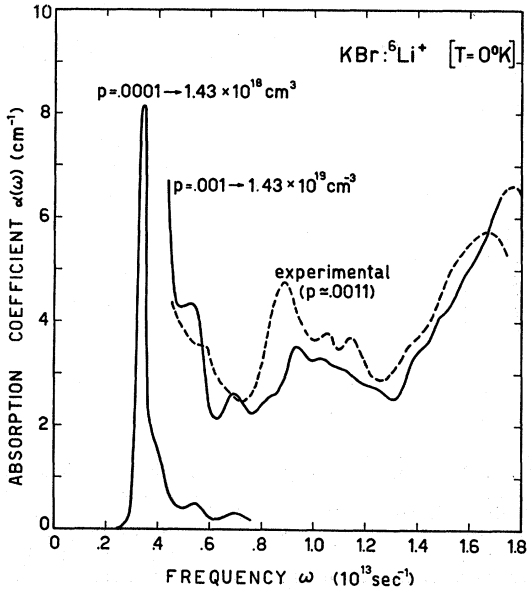

FIG. 7. Calculated (solid line) and experimental (broken line) IR absorption coefficient for KBr: $^6Li^+$ at 0°K in the low-frequency region. The resonance peak is reported for a concentration of defects 10 times smaller. In the resonance region the experimental points fall on the theoretical line.

they depend only on λ, these plots hold for all positive defects in KBr. By using the fitted values of $\tilde{f}^*$ for $^6Li^+$ and Ag^+, we see that four resonances (two of the Γ_1 and two of the Γ_{12} type) are induced by Li^+, while no resonance is induced by Ag^+. The resonances induced by Li^+ have been recently observed by Pohl[25] in thermal conductivity experiments, and the agreement with our resonance frequencies is very good. Notice that such resonances are activated in KBr by those impurities for which $-1.25\leq f^*/(\tilde{f}^*-f^*)\leq1.43$, i.e., for a large weakening or strengthening of the force constant. As regards Γ_1 and Γ_{12} local modes, it appears that only an extremely high (and probably unphysical) positive value of $\tilde{f}^*$ could produce a Raman-active local mode. However, notice that our definition of f^*, which is probably correct for Γ_{15} modes, could not apply equally well to Γ_1 or Γ_{12} modes.

We now use the fitted values of λ to evaluate the frequency-dependent absorption coefficient of KBr:$^6Li^+$ and KBr:Ag^+, as given by Eq. (61) (see Fig. 7). In order to make a significant comparison with the experimental data, we must note that the "tail" coming from the *Reststrahlen* is minimized at $T=0$°K, but for a finite concentration p of defects it cannot be subtracted from the total spectrum because the *Reststrahl* itself is influenced by the finite concentration of defects. However, for the values of p we have used here the spectra do not seem to differ substantially from the one-defect spectra, except for $\omega\geq1.5\times10^{13}$ sec^{-1} where the *Reststrahl*

[25] R. O. Pohl, in Lectures on Elementary Excitations and Their Interactions in Solids, NATO Advanced Study Institute, Cortina, 1966 (to be published).

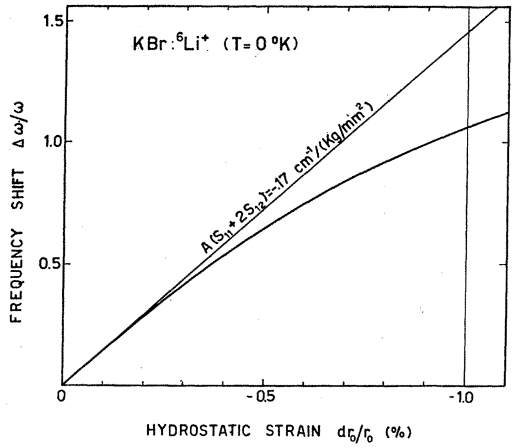

FIG. 8. Resonance frequency shift versus hydrostatic strain in KBr: $^6Li^+$. The first derivative of this function is proportional to the hydrostatic coefficient $A(s_{11}+2s_{12})$ (see Ref. 23). Note the nonlinearity of $\Delta\omega_R/\omega_R$ versus $\Delta r_0/r_0$, which causes the hydrostatic coefficient deduced from the shift at 1% strain, as in Ref. 23, to be quite smaller than that deduced from the shift at vanishing strain.

broadening becomes sensible. Figure 7 shows that fairly good agreement exists between calculated and experimental absorption spectra, particularly at resonance; also the agreement between theoretical and experimental absorption amplitudes is remarkable. Thus it seems that the structured spectrum in the region 0.4×10^{13} $\text{sec}^{-1}<\omega<1.6\times10^{13}$ sec^{-1} essentially reflects the shape of the normal-mode Γ_{15} frequency density, while the resonance at $\omega=1.24\times10^{13}$ sec^{-1} is really very broad and unobservable.

As remarked above, the low-lying resonant modes are very sensitive to a variation of λ. Elsewhere,[23] we have discussed how to produce such a variation (and therefore a large frequency shift or splitting of the peak), and we have given estimates of the hydrostatic coefficient for the resonance frequency of some doped crystals. In Fig. 8 we show the calculated resonance frequency shift for an increasing hydrostatic strain and in Fig. 9 we show the effect of a -0.6% hydrostatic strain on the resonance absorption in KBr:$^6Li^+$. The change in shape is very remarkable; however, the broadening seems to be entirely due to the large shift towards a more dense region of the phonon spectrum, the amplitude factor, as defined in Ref. 23, being very close to unity. On the other hand, the structures due to the host-lattice dynamics remain essentially unchanged.

As concerns the dependence of the resonance frequency on ϵ, it is known that replacement of $^6Li^+$ with $^7Li^+$ in KBr yields an isotope shift of the frequency equal to -10%.[9] It is surprising that simplified dynamical models in which long-range forces are neglected[9,10] account quite well for this isotope shift, while the present calculations, based on the DD model, predict an isotope shift not exceeding -5%. However, we have some evidence that the strong anharmonicity, mainly fourth-order, of the low-frequency resonant mode is able to produce by itself, even at $T=0$°K, an isotope shift of the same sign and order of magnitude as the harmonic shift.

Let us now consider the absorption spectrum induced by Ag^+ (Fig. 10), as obtained from (61) after fitting $\tilde{f}^*$ to the resonance peak. Poor agreement is found between the experimental and the theoretical peak shape, particularly at high concentration, while no correspondence exists between the theoretical predictions

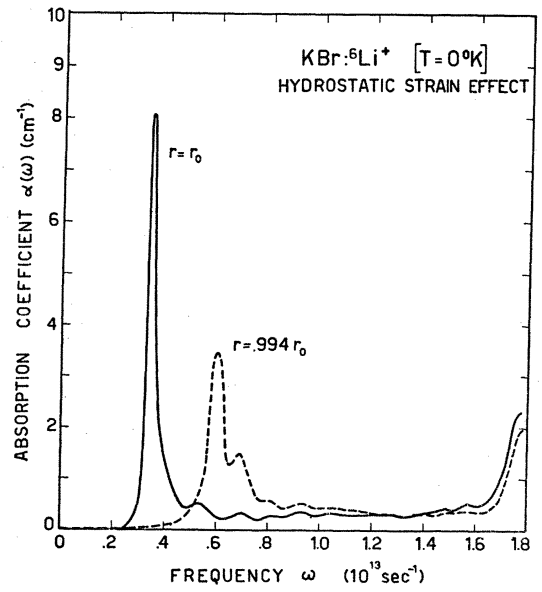

FIG. 9. The effect of a hydrostatic strain on the absorption spectrum of KBr:$^6Li^+$.

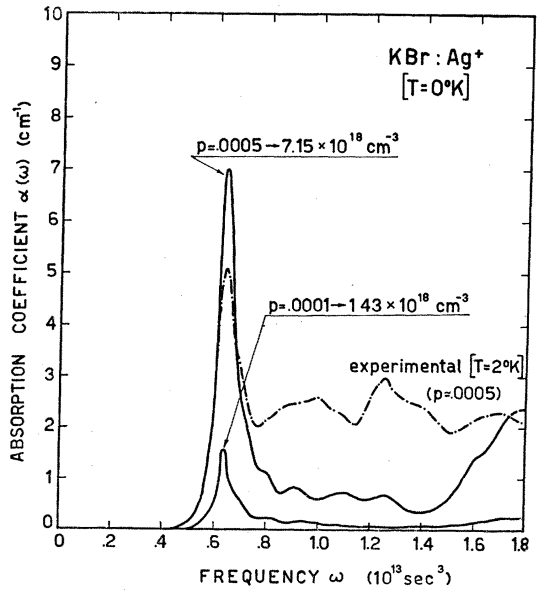

FIG. 10. Calculated (solid line) and experimental (broken line) IR absorption coefficient for KBr:Ag^+ at 0°K for two values of defect concentration.

and the observed structures at higher frequencies. However, this disagreement is no surprise in principle, since Ag^+ is expected to induce a more extended perturbation than that induced by Li^+, which has a tightly bound core structure. Calculation based on a model of $\mathbf{\Lambda}(\omega^2)$ including also the perturbation on 2nd neighbors should be able to test the present interpretation of such discrepancies. A completely different interpretation is proposed below for the experimental observations. However, we have used the KBr:Ag^+ absorption peak to show (Fig. 11) the effects of an increasing concentration on the band shape, according to Eq. (61). In Fig. 11 the intensity of the bands corresponding to $p=10^{-3}$ and $p=10^{-2}$ are reduced by a factor of 10 and 100, respectively, in order to allow for a better comparison. Up to $p=10^{-2}$, which should be considered a large value with respect to the reliability of the low-concentration approximation, shall changes in shape occur. Indeed, the shift in frequency seems to be detectable, and agrees with the measurements of NaCl highly doped with AgCl (from $p=2.3\times10^{-3}$ to $p=2.3\times10^{-2}$) by Weber[26], who observed a small shift towards lower frequencies as p increases. This nonlinearity in p comes mainly from the optical contribution $T_{OO}(z)$ [see Eq. (57)] while the acoustic terms $T_{AO}(z)$ and $T_{AA}(z)$ are found to be negligible.

B. Results for the Change of Force Constant

Suitably chosen phenomenological potentials are used in the *a priori* calculations of the short-range interaction. When these potentials have been fitted to certain crystal properties (namely, the lattice constant and the compressibility), their reliability is good over the whole range of validity of the corresponding equation of state with respect to a variation in temperature and pressure. From this point of view, simple potentials, such as the Born-Mayer[27], Pauling,[27] or Lennard-Jones[28] potentials, have been proven to be quite satisfactory. However, these potentials can be used less safely to predict the interaction between ions which are much displaced from their "equilibrium" distance, i.e., the interionic distance on which the potentials themselves were fitted. Since any *a priori* calculation of $\tilde{f}^*$ would meet this uncertainty, we want to investigate here the consistency between calculation and fitting to IR data. In the Born-Mayer form the n.n. potential is

$$\varphi^{(R)}(r)=c_{+-}e^{(r_++r_--r)/\rho}, \tag{70}$$

where $r_\pm$ is the ionic radius, ρ is the screening radius, and c_{+-} is the Pauling coefficient.[27] The two free parameters ρ and $c_{+-}\exp(r_++r_-/\rho)$ are deduced by fitting the crystal potential

$$\varphi(r)=-\alpha_M e^2/r+6\varphi^{(R)}(r) \tag{71}$$

to the zero-temperature lattice parameter r_0 and compressibility. In Fig. 12 we plot $\tilde{f}^*$ for KBr:Li^+ as a function of the n.n. distance $\tilde{r}$ (or the relative relaxation $\xi=\tilde{r}/r_0-1$) for two different values of the effective ionic change which enters the deformation-dipole term: $\tilde{e}^*/e=0.70$ refers to LiBr, and $\tilde{e}^*/e=0.76$ to KBr.[18] The fitted $\tilde{f}^*$ and the elastic relaxation calculated according to Fukai's method[29] are also indicated.

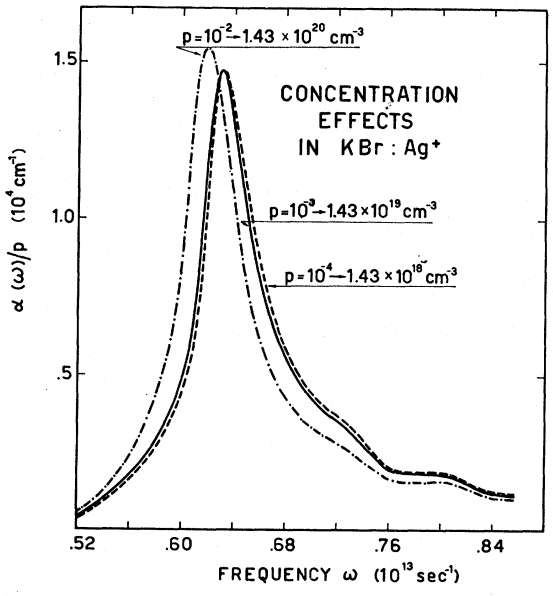

FIG. 11. Concentration effect on the absorption peak of KBr:Ag^+. The absorption coefficient at different concentrations has been divided by the concentration itself in order to make easier the detection of the concentration effect as p is increased.

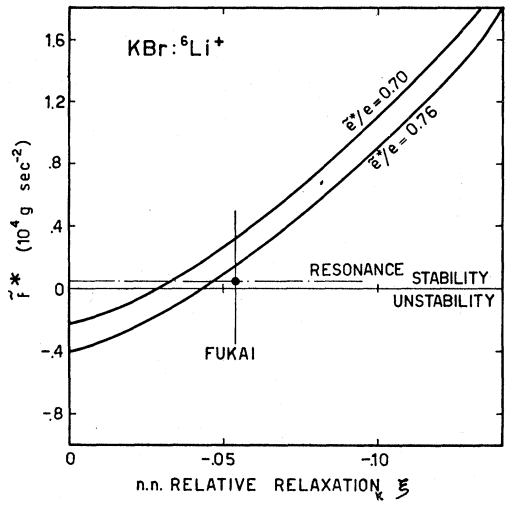

FIG. 12. The effective n.n. force constant of Li^+ in KBr from a Born-Mayer potential plotted versus n.n. elastic relaxation for two different values of the local effective charge: $\tilde{e}^*=0.70e=e^*$(LiBr) and $\tilde{e}^*=0.76e=e^*$(KBr).

[26] R. Weber, Phys. Letters **12**, 311 (1964).

[27] F. G. Fumi and M. P. Tosi, J. Phys. Chem. Solids **25**, 31 (1964); M. P. Tosi and F. G. Fumi, *ibid.* **25**, 45 (1964).

[28] M. N. Sharma and M. P. Madan, Indian J. Phys. **38**, 231 (1964).

[29] Y. Fukai, J. Phys. Soc. Japan **18**, 1413 (1963).

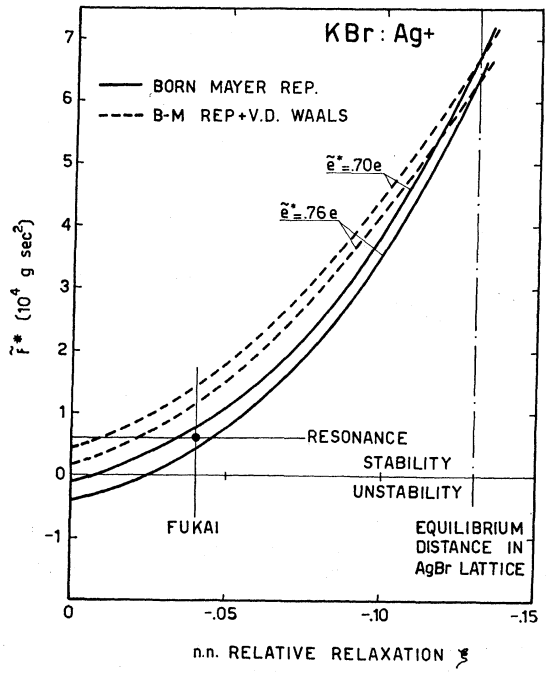

FIG. 13. The effective n.n. force constant of Ag^+ in KBr plotted versus n.n. elastic relaxation from a potential including or not including van der Waals terms. Two values of the local effective charge are used: $\tilde{e}^*=0.70e=e^*(\text{AgBr})$ and $\tilde{e}^*=0.76e=e^*(\text{KBr})$.

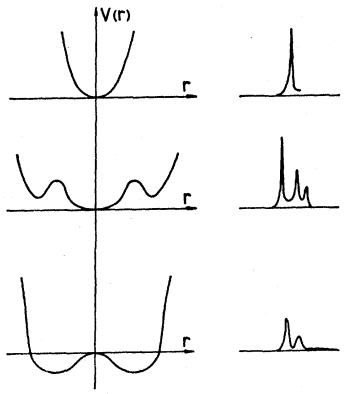

FIG. 14. Qualitative predictions for the shape of the absorption coefficient with respect to the shape of the impurity potential well. For an impurity equilibrium position displaced from the lattice site, the resonance splits into a doublet whose strengths are in the ratio 2:1. The assignment of experimental peaks to some shape of the potential well could be tested by stress experiments.

For realistic values of ξ, the quantity $\tilde{f}^*$ is positive, i.e., the lithium ion is stable at its lattice site; instability becomes possible for small values of the relaxation, as pointed out recently.[30] In this case, because of the displaced equilibrium position of the defect, anisotropy occurs in the $\mathbf{\Lambda}$ matrix, which produces a splitting of the resonance peak. As was recently pointed out from an experimental study by Nolt and Sievers,[24] for Li^+ in KBr this does not seem the case. Figure 13 shows analogous plots for KBr:Ag^+. In fitting the Ag^+-Br^- interaction potential to the low-temperature experimental data, the van der Waals (vdW) terms $-c/r^6$ $-d/r^8$ must be included; indeed, the plots of $\tilde{f}^*$ so obtained differ remarkably from those in which vdW terms are neglected. It is interesting to note that the inclusion of vdW terms increases the stability of silver at its lattice site. However, the low ionicity of the bond and the higher polarizability of silver could create some other equilibrium positions for Ag^+ at displaced sites in the sense expressed by Matthew[30] and described in Fig. 14. In this case some otherwise unexplained absorption peaks would be expected.

Examining these plots, we note in general that as far as the elastic relaxation and overalp interaction are known, consistency is found between the calculated and the fitted change in force constant, even if $\tilde{f}^*$ depends too strongly on the elastic relaxation, effective charge, and choice of interionic potential itself to allow any reliable prediction. However, there is some evidence that the local change in effective charge should be small (i.e., $\tilde{e}^*$ approaches the host-lattice effective charge) and the true elastic relaxation slightly larger, in absolute value, than that which fits the experimental $\tilde{f}^*$. In fact, if n.n. ions relax inwardly, the interaction between defect and n.n. is hardened while all the other n.n. force constants are softened by the relaxation field, which covers the whole remaining crystal. Analogously for $\xi>0$; thus the local relaxation effect should be partially compensated.

APPENDIX

The most general form of the frequency-independent perturbation $\mathbf{\Lambda}_0$ on n.n. interaction should include the change in noncentral force constant λ'. For a NaCl-type lattice the complete form of the symmetric matrix $\mathbf{\Lambda}_0$ is given by

$$(000|\mathbf{\Lambda}_0|000)=\begin{vmatrix}\lambda+2\lambda' & 0 & 0\\ 0 & \lambda+2\lambda' & 0\\ 0 & 0 & \lambda+2\lambda'\end{vmatrix};$$

$$\chi^{1/2}(000|\mathbf{\Lambda}_0|100)=\chi^{1/2}(000|\mathbf{\Lambda}_0|-100)=-(100|\mathbf{\Lambda}_0|100)=\chi\begin{vmatrix}\tfrac{1}{2}\lambda & 0 & 0\\ 0 & \tfrac{1}{2}\lambda' & 0\\ 0 & 0 & \tfrac{1}{2}\lambda'\end{vmatrix}\text{ and cyclic permutations;}$$

$$(l\kappa|\mathbf{\Lambda}_0|l\kappa)=0\text{ otherwise.}\qquad\text{(A1)}$$

All the irr.rep. of the point group O_h which are associated with the 21-dimensional system of the impurity plus its

[30] J. A. D. Matthew, Solid State Commun. 3, 365 (1965); G. J. Dienes, R. D. Hatcher, R. Smoluchowski, and W. Wilson, Phys. Rev. Letters 16, 25 (1966).

six nearest neighbors contribute to the perturbed normal-mode spectrum. One finds

$$\begin{aligned}
&(\Gamma_1|\mathbf{\Lambda}|\Gamma_1) = \chi\lambda/2 \quad (1\text{-fold})\\
&(\Gamma_{12}|\mathbf{\Lambda}|\Gamma_{12}) = \chi\lambda/2 \quad (2\text{-fold})\\
&(\Gamma_{15}'|\mathbf{\Lambda}|\Gamma_{15}') = \chi\lambda'/2 \quad (3\text{-fold})\\
&(\Gamma_{15}|\mathbf{\Lambda}|\Gamma_{25}) = \chi\lambda'/2 \quad (3\text{-fold})\\
&(\Gamma_{25}'|\mathbf{\Lambda}|\Gamma_{25}') = \chi\lambda'/2 \quad (3\text{-fold})
\end{aligned}$$

$$(\Gamma_{15}|\mathbf{\Lambda}|\Gamma_{15}) = \begin{vmatrix} \epsilon\omega^2+\lambda+2\lambda' & -(\chi/2)^{1/2}\lambda & -\chi^{1/2}\lambda' \\ -(\chi/2)^{1/2}\lambda & (\chi/2)\lambda & 0 \\ -\chi^{1/2}\lambda' & 0 & (\chi/2)\lambda' \end{vmatrix} . \quad \text{(3-fold)} \tag{A2}$$

Only the Γ_{15}-resonance modes contribute to the dipole IR absorption, while the resonances of Γ_1, Γ_{12}, Γ_{15}', and Γ_{25}' are involved in the first-order Raman scattering induced by the impurity. The resonance denominators for each irr.rep. can be easily written down in terms of some integrals in the Brillouin zone. In particular we have

$$D^{(\Gamma_{15})}(z) = \det \begin{vmatrix} 1+(\epsilon\omega^2+\lambda+2\lambda')\mathcal{G}_1 - \chi^{1/2}\lambda\mathcal{G}_2 - 2\chi^{1/2}\lambda'\mathcal{G}_7 & -(\chi/2)^{1/2}\lambda\mathcal{G}_1+\chi/2^{1/2}\lambda\mathcal{G}_2 & -\chi^{1/2}\lambda'\mathcal{G}_1+\chi\lambda'\mathcal{G}_7 \\ 2^{1/2}(\epsilon\omega^2+\lambda+2\lambda')\mathcal{G}_2 - (2\chi)^{1/2}\lambda\mathcal{G}_3 - 2\chi^{1/2}\lambda'\mathcal{G}_8 & 1-\chi^{1/2}\lambda\mathcal{G}_2+\chi\lambda\mathcal{G}_3 & -(2\chi)^{1/2}\lambda'\mathcal{G}_2+\chi\lambda'\mathcal{G}_8 \\ 2(\epsilon\omega^2+\lambda+2\lambda')\mathcal{G}_7 - (2\chi)^{1/2}\lambda\mathcal{G}_8 - 2\chi^{1/2}\lambda'\mathcal{G}_9 & -(2\chi)^{1/2}\lambda\mathcal{G}_7+\chi\lambda\mathcal{G}_8 & 1-2\chi^{1/2}\lambda'\mathcal{G}_7+\chi\lambda'\mathcal{G}_9' \end{vmatrix} , \tag{A3}$$

where $\mathcal{G}_\mu^{\pm}(z)$ ($\mu=7, 8, 9$) are defined according to Eq. (21), with

$$\begin{aligned}
j_7^{\pm}(z) &= e_x(\pm|\mathbf{q},s)e_x(\mp|\mathbf{q},s)\cos(2\pi r_0 q_y) ,\\
j_8^{\pm}(z) &= e_x^2(\mp|\mathbf{q},s)\cos(2\pi r_0 q_x)\cos(2\pi r_0 q_y) ,\\
j_9^{\pm}(z) &= e_x^2(\mp|\mathbf{q},s)\{\cos^2(2\pi r_0 q_y)+\cos(2\pi r_0 q_y)\cos(2\pi r_0 q_z)\} .
\end{aligned} \tag{A4}$$

The change in noncentral force constant affects the Γ_{15} irr.rep. (we now have a 3×3 matrix) and introduces some new characteristic odd-parity normal modes of Γ_{15}', Γ_{25}, and Γ_{25}' type, while it has no influence on Γ_1 and Γ_{12} normal modes. However, it can be shown that realistic values of λ' are able neither to excite resonant or localized Γ_{15}', Γ_{25}, and Γ_{25}' modes, nor to affect appreciably the Γ_{15} resonance conditions.

PHYSICAL REVIEW VOLUME 155, NUMBER 3 15 MARCH 1967

Electromechanical Behavior of Single-Crystal Strontium Titanate

G. RUPPRECHT
Borders Electronics Research Corporation, Waltham, Massachusetts
AND
W. H. WINTER
Research Division, Raytheon Company, Waltham, Massachusetts

(Received 26 October 1966)

A study of electrostriction in strontium titanate provides evidence that $SrTiO_3$ is not perfectly cubic. It exhibits a small but noticeable piezoelectric effect whose temperature and field dependence is $E/(T-T_a)$, whereas the electrostrictive effect was found to vary as $E^2/(T-T_c)^2$. T_a and T_c are the temperature of the phase transition (102.5°K) and the Curie temperature (41°K), respectively. The results of an extensive study of the compliance constant s_{11} above and below the phase transition are reported and are combined with previously reported data to yield a complete set of elastic coefficients $c_{ik}(T,E)$ or $s_{ik}(T,E)$ as a function of temperature and externally applied electric field E. An accurate determination of the transition temperature as a function of electric field provides the basis for a possible check on a recent explanation of the phase transition by Cowley.

I. INTRODUCTION

IT is known that $SrTiO_3$ is of the cubic perovskite structure with symmetry class $m3m$. It has been noticed, however, that a phase transition of at least second order takes place at about 100°K, which manifests itself most strikingly as an abrupt change of the elastic constants,[1] a gradual splitting of the EPR spectrum in crystals doped with magnetic impurities,[2] a change of the c/a ratio to 1.00056,[3,4] and a decrease of amplitude of the nuclear magnetic resonance of Sr^{87}.[5]

Based upon the observation of birefringence and

[1] R. O. Bell and G. Rupprecht, Phys. Rev. **129**, 90 (1963).

[2] L. Rimai and G. A. de Mars, Phys. Rev. **127**, 702 (1962).

[3] R. S. Krogstad and R. W. Moss, Bull. Am. Phys. Soc. **7**, 192 (1962).

[4] F. W. Lytle, J. Appl. Phys. **35**, 2212 (1964).

[5] M. J. Weber and R. R. Allen, J. Chem. Phys. **38**, 726 (1963).